hydrate crystals are first observed. With D_o as a fitting parameter, I found that D_o = 2100 cm^2 s^{-1} gave acceptable fits to both the Vostok data and the Byrd data (9) on bubble concentration as a function of depth.

Figure 2 displays values of $1/\lambda_{bub} \equiv n\pi r^2$, the reciprocal of the bubble-to-bubble scattering length, as a function of depth, z, for Vostok, Byrd, and South Pole. The experimental points use data on bubble concentration, $n(z)$, and radius, $r(z)$, for Vostok and for Byrd. The data for South Pole are from in situ light scattering at depths of 800 to 1000 m (15). The curves show the results of applying the diffusion model to the three sets of data. The value for $n(t)$ is calculated from Eq. 2, taking $a = a_o$, the mean radius at the dissociation pressure. The observed values are a_o = 68 μm for Vostok and 130 μm for Byrd. In the absence of data on a_o for the South Pole, I assumed the same value as for Vostok, because those two sites have similar elevations, surface temperatures, atmospheric pressures, and hydrate dissociation pressures (see Fig. 1), which are rather different from those at Byrd. To compute the curve for $1/\lambda_{bub}$, I assumed that $r = a_o (P_e/P)^{1/3}$ due to hydrostatic pressure. The fits to the data for Vostok and Byrd are quite good and lend confidence to the predicted dependence of $1/\lambda_{bub}$ on depth for the South Pole (26).

The diffusion-growth model provides a solution to the puzzles listed in the introduction. The reason that bubbles do not all convert into air hydrate crystals at the phase transition pressure, and the reason for the great range of depths at which both air hydrate crystals and bubbles coexist, is that the time required for water molecules to diffuse through a growing shell of air hydrate at ambient ice temperature is extremely long. The diffusion coefficient for water in air hydrate, $D(T) = D_o\exp(-0.9/kT)$, with D_o = 2100 cm^2 s^{-1}, is orders of magnitude smaller than for self-diffusion in hexagonal ice. For example, at −46°C, the temperature of South Pole ice at a depth of 1 km, $D = 2.2 \times 10^{-17}$ cm^2 s^{-1} for water in air hydrate, whereas $D = 2.65 \times 10^{-13}$ cm^2 s^{-1} for water in hexagonal ice. The reason for the apparent lack of organization of the data on bubble disappearance in Fig. 1 is that the depth is the wrong variable to use. Because of large variations in snow accumulation rate from one polar site to another, depth is not universally related to time. Only when data are plotted on a graph of time versus reciprocal of temperature does the correlation become clear. When applied to laboratory data on the rate of decrease of concentration of bubbles in ice near the melting point (19), the model gives results consistent with the data.

The model predicts that in deep ice at the South Pole, the bubble-to-bubble scattering length is ~6 m at a depth of 1300 m, 20 m at 1400 m, and 130 m at 1500 m. For an AMANDA phototube spacing of 20 m, bubbles will cease to degrade imaging at depths greater than ~1400 m.

REFERENCES AND NOTES

1. S. L. Miller, *Science* **165**, 489 (1969).
2. For Dome C, see C. Ritz, L. Lliboutry, C. Rado, *Ann. Glaciol.* **3**, 284 (1982).
3. For Dye 3, see D. Dahl-Jensen and S. J. Johnsen, *Nature* **320**, 250 (1986).
4. For Byrd and Camp Century, see W. F. Budd and N. W. Young, in *The Climatic Record in Polar Ice Sheets*, G. de Q. Robin, Ed. (Cambridge Univ. Press, Cambridge, 1983), p. 150.
5. For Vostok, see C. Ritz, *Ann. Glaciol.* **12**, 138 (1989).
6. A model for temperature versus depth at the South Pole was developed by B. Koci (unpublished material).
7. AMANDA collaboration, *J. Glaciol*, in press.
8. N. I. Barkov and V. Ya. Lipenkov, *Mat. Glyatsiol. Issled.* **51**, 178 (1984).
9. A. J. Gow and T. Williamson, *J. Geophys. Res.* **80**, 5101 (1975).
10. V. Ya. Lipenkov, *Mat. Glyatsiol. Issled.* **65**, 58 (1989).
11. T. Uchida, T. Hondoh, S. Mae, V. Ya. Lipenkov, P. Duval, *J. Glaciol.* **40**, 79 (1994).
12. H. Shoji and C. C. Langway Jr., *Nature* **298**, 548 (1982).
13. ______, *J. Phys. (Paris)* **48**, 551 (1987).
14. S. Barwick *et al.*, *J. Phys. G Nucl. Part. Phys.* **18**, 225 (1992).
15. AMANDA collaboration, *Science*, in press.
16. T. Uchida *et al.*, *in Proceedings of the International Conference on the Physics and Chemistry of Ice*, N. Maeno and T. Hondoh, Eds. (Hokkaido Univ. Press, Sapporo, Japan, 1992), pp. 121–125.
17. T. Uchida *et al.*, *in Fifth International Symposium on Antarctic Glaciology*, in press.
18. K. Goto, T. Hondoh, A. Higashi, *Jap. J. Appl. Phys.* **25**, 351 (1986).
19. T. Ikeda, T. Uchida, S. Mae, *Proc. NIPR Symp. Polar Meteorol. Glaciol.* **7**, 14 (1993).
20. N. H. Fletcher, *J. Chem. Phys.* **29**, 572 (1958).
21. W. K. Burton, N. Cabrera, F. C. Frank, *Philos. Trans. R. Soc. London Ser. A* **243**, 299 (1951).
22. Self-diffusion in ice occurs by diffusion of interstitial water molecules rather than by vacancies (18).
23. An alternative possibility, that air molecules diffuse through the air hydrate shell and convert ice to air hydrate at the bubble boundary, is ruled out experimentally. Uchida *et al.* (16, 17) observed that air hydrate crystals grow inwardly, causing bubbles to shrink in size and eventually disappear.
24. J. Crank, *The Mathematics of Diffusion* (Clarendon, Oxford, 1975).
25. This assumes that the vapor pressure of water at the surface of an air hydrate crystal is much smaller than at the surface of an ice crystal.
26. An alternative procedure is to fix D_o at 1.2 cm^2 s^{-1}, the same value for diffusion of water in air hydrate as in ice, and to treat E_s as a fitting parameter. Doing this leads to acceptable fits to the Vostok and Byrd data but with E_s = 0.75 eV, which is outside the standard error claimed in (11). The resulting curves for $1/\lambda_{bub}$ for Vostok, Byrd, and South Pole are similar to those calculated with D_o = 2100 cm^2 s^{-1}, E_s = 0.9 eV. The conclusion is that the present data do not permit determination of both D_o and E_s independent of laboratory data.

27. Supported in part by National Science Foundation grant PHY-9307420.

25 October 1994; accepted 20 January 1995

Dike Injection and the Formation of Megaplumes at Ocean Ridges

Robert P. Lowell and Leonid N. Germanovich

A simple hydrologic model of seawater circulation at ocean ridge axes implies that the transient occurrence of large volumes of buoyant, heated water in the oceanic water column (megaplumes) can be attributed to the emplacement of dikes in oceanic crust. For dikes to generate megaplume flow, the permeability of both the recharge areas and the upflow zone must be greater than that required for ordinary black smokers. An increase in permeability in the upflow zone by several orders of magnitude results from dike emplacement, and megaplume discharge ceases as the dike cools. Vigorous black smoker venting may not persist very long at a megaplume site after the event occurs.

Megaplumes (or event plumes) appear to be sudden, short-lived hydrothermal events on the sea floor (Fig. 1). Even though the temperature of the water in megaplumes is only slightly higher than in the ambient ocean (by up to 0.25°C), their large volume indicates the liberation of ~10^{17} J of heat (1, 2). Baker *et al.* (2) argued that the geometry of the plume and its particulate content are indicative of an event lasting 2 to 20 days. The heat and mass fluxes are thus two to three orders of magnitude greater than typical, quasi-steady black smoker venting. A simple heat balance shows that roughly 0.01 km^3 of magma can provide the heat content of a megaplume; however, the chemical constituents of megaplumes (2, 3) and the rise height of the plume appear to make direct interaction between seawater and an extrusive lava flow an unlikely mechanism for megaplume generation (2). Nevertheless, observations of recent lava flows in the vicinity of the megaplumes observed

R. P. Lowell, School of Earth and Atmospheric Sciences, Georgia Institute of Technology, Atlanta, GA 30332, USA.

L. N. Germanovich, School of Petroleum and Geological Engineering, University of Oklahoma, Norman, OK 73019, USA.

on the northern Cleft segment of the Juan de Fuca Ridge in the northeast Pacific (4) and the detection of essentially simultaneous seismicity, basaltic lava flows, and megaplumes on the CoAxial segment Juan de Fuca Ridge in the summer of 1993 (3, 5, 6) lend credence to the idea that megaplumes are associated with lateral dike propagation (7).

In this report we present a simple hydrologic model of seawater circulation at ridge axes and show that the emplacement of a dike into the shallow oceanic crust can alter the hydrologic and thermal regime in a manner consistent with the formation of a megaplume. Our model differs from others (8, 9) that relate megaplumes to episodic variations in normal black smoker systems. For example, Cann and Strens (8) proposed that rupture of an impermeable cap above a normal, active black smoker system by hydraulic fracturing produces a megaplume, whereas Cathles (9) suggested that megaplume emissions result from episodic flow variations along the margins of a large, axial magma chamber that is driving active black smoker venting. These earlier models are incomplete because they do not relate megaplumes to magmatic events. Moreover, there is no evidence that black smoker activity existed prior to the megaplumes on the CoAxial segment (10), and there is considerable evidence that high-temperature venting after a megaplume may decline rapidly (7). Our model, on the other hand, directly invokes dike injection to provide both the hydrological conditions necessary for a megaplume as well as the necessary thermal perturbation. The model does not require the prior existence of a black smoker venting system and is consistent with observations that hydrothermal activity may wane rapidly after the megaplume. Moreover, our model indicates that for megaplume flow to occur after dike injection, the initial permeability in the recharge zone must exceed $\sim 10^{-12}$ m^2. Thus, not all dike injections will necessarily generate megaplumes. The model is also consistent with data on ^{3}He/heat ratios (10–12) and metal content of megaplume fluids (2, 3).

We assume that fluid flow is along a single pass through the crust (Fig. 2). We consider both cross-axis and along-axis flow because it is uncertain whether the recharge area is significantly larger than the discharge area (Fig. 2A) or whether the circulation is controlled by predominantly along-axis flow (Fig. 2B), in which case the discharge and recharge areas may be of about the same size.

For typical black smoker flows, we assume that Darcy's law holds. Then, the total mass flux Q reflects the ratio of the pressure head driving the flow to the total flow resistance in the upflowing (u) and downflowing (d) limbs. Thus

$$Q = \frac{\frac{2}{3}\Delta\rho g}{\frac{\nu_d}{K_d A_d} + \frac{\nu_u}{K_u A_u}} \tag{1}$$

where $\Delta\rho$ is the density difference between the descending and ascending limbs of the convection cell, g is the acceleration due to gravity, ν is the kinematic viscosity, K is the permeability, and A is the area. The factor of 2/3 arises from assuming that the flow resistance in the horizontal limb is equal to the average of that in the upflow and downflow limbs.

For black smoker venting, $\Delta\rho g \approx 5000$ kg m^{-2} s^{-2}. For a temperature of $\sim$350°C and a power output of $\sim$250 MW, which is typical of many vent fields (13), $Q \sim 100$ kg s^{-1}. In the downwelling fluid, $\nu_d = 10^{-6}$ m^2 s^{-1}, whereas in the hotter upwelling fluid, $\nu_u = 10^{-7}$ m^2 s^{-1} because the viscosity decreases with increasing temperature (14). The area of vent fields varies considerably (13), but for convenience, we use $A_u \sim 10^4$ m^2, corresponding to an area a few tens of meters across at the ridge axis and extending for a few hundred meters along the axis. From these parameters and in the limit that all the flow resistance is in the upflow (discharge-dominated flow), we find from Eq. 1 that $K_u > 3 \times 10^{-13}$ m^2. This is a lower limit for K_u. By taking the limit that all the flow resistance is in the downflow (recharge-dominated flow), we can place lower limits on the value of K_d. Choosing $A_d = 10^6$ m^2 (Fig. 2A) gives $K_d > 3 \times 10^{-14}$ m^2, whereas choosing $A_d = 10^4$ m^2 (Fig. 2B) gives $K_d > 3 \times 10^{-12}$ m^2. Thus, for ordinary black smoker flow, the permeability of the recharge zone may be either greater than or less than that of the discharge zone, depending on the area of the recharge zone.

A megaplume event such as occurred over the Juan de Fuca Ridge in the northeast Pacific is thought to correspond to the release of $\sim 10^8$ m^3 at a temperature $T \approx 350°$ to 400°C over the course of a few days ($\sim 10^6$ s) (1). Such an event requires a mass flux $Q = 2.5 \times 10^4$ kg s^{-1} (along each dike wall in our model). For megaplume flow, we use a model of permeability based on the turbulent upflow through a set of planar parallel cracks located near ($\sim$1 m) the dike wall (15). This model is advocated by the fact that the rock brecciated by the dike propagation is probably adjacent to the dike walls (16); besides, dike parallel joints are expected to accompany dike emplacement (16–18). The analogous single-pass hydrologic model is then

$$\Delta\rho g = \frac{2\nu_d Q}{K_d A_d} + \frac{f Q^2}{\rho_u n L^2 D^3} \tag{2}$$

where f is the friction factor, n is the number of cracks, D is the width of an individual crack, and L is the length of the discharge zone along strike. The factor of 2 arises from assuming that the resistance in the horizontal limb equals that in the recharge limb. If we again take the limit of recharge-dominated flow, then $K_d > 10^{-11}$ m^2 for $A_d = 10^6$ m^2, whereas $K_d > 10^{-9}$ m^2 if $A_d = 10^4$ m^2. Thus, for a megaplume to occur, the permeability of the recharge zone must be greater than that required for ordinary black smoker flow. Thus, if a megaplume occurs in a currently active black smoker system, the black smoker system must be discharge-dominated. If we assume that flow is discharge-dominated, $D > 0.0017$ m for a discharge length L of 10^4 m (19), a friction factor f of 0.02 (20), and 10 cracks per meter. In this case, the effective permeability of the upflow zone $K_u \approx D^3/(12h) > 4 \times 10^{-9}$ m^2, where h is the mean crack spacing. If $n = 100$, then $D > 8 \times 10^{-4}$ m and, again, $K_u \approx 4 \times 10^{-9}$ m^2.

Megaplume flow therefore seems to require more restrictive hydrologic conditions than ordinary black smokers. Not only must the recharge permeability be greater than is necessary for black smoker flow, but also the permeability of the upflow zone must be several orders of magnitude greater than for

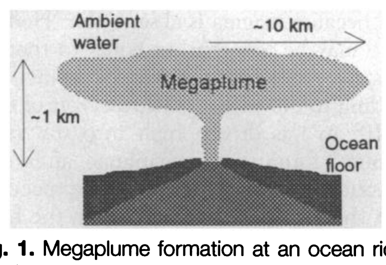

Fig. 1. Megaplume formation at an ocean ridge axis (the vertical scale is exaggerated).

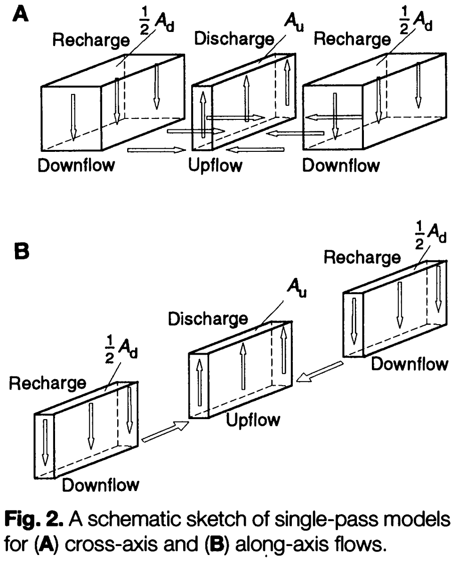

Fig. 2. A schematic sketch of single-pass models for (**A**) cross-axis and (**B**) along-axis flows.

ordinary black smokers. Therefore, if a black smoker system existed before the emplacement of a dike, it is not necessary that a megaplume occurs. It may occur only if the recharge permeability during black smoker flow is sufficient. Moreover, the formation of a megaplume requires that the permeability near the dike walls increase by several orders of magnitude to bring the discharge permeability to the required level.

We suggest that the high permeability in the upflow zone can be associated with the mechanics of dike injection. At the largest scales, dike injection tends to produce cracks parallel to the dike in adjacent country rock (*17*, *18*). The newly created joints themselves can dramatically increase permeability in the direction of dike propagation. At a smaller scale, perhaps within one dike thickness, that is, ~1 to 10 m, dike propagation can brecciate the rock (*16*). Finally, even subsidiary permeability can increase in the rock adjacent to the dike as ascending thermal waters heat fluid-filled cracks (*21*). For land-based systems, superheated steam ascending along the dike walls and heating the country rock can lead to the propagation of isolated microcracks, increasing their length by more than an order of magnitude (*21*). An analogous situation occurs in sea-floor systems (*22*). A quantitative analysis of the permeability enhancement that might occur upon the injection of the dike is a difficult problem. At this point in our understanding, we, as have others (*1*, *4*, *8*, *9*), can only advocate the necessity for such permeability increases in order for megaplumes to occur.

In our model, heat as well as permeability is furnished by the dike. To obtain an estimate of how long heat from a dike might drive high-temperature megaplume flow, we consider the thermal problem of heat transfer from the dike to the rapidly ascending fluid near the dike wall (Fig. 3). We consider the dike to be initially at a temperature $T_0 =$ 1200°C and that fluid enters the cracked zone at the base at a temperature $T_1 =$ 200°C. Assuming thermal equilibrium between the fluid near the dike and the solidified dike, neglecting the latent heat of the dike, and assuming that the dike is a half-space, the temperature of the fluid at a distance x along the dike is estimated by (*23*)

$$T(x, t) = T_m + (T_1 - T_m)\mathrm{erfc}\left[\frac{\lambda L x}{2sQ(at)^{1/2}}\right] \qquad (3)$$

where $T_m = (T_0 + T_1)/2$ is the mean temperature of the wall, λ and a are the thermal conductivity and diffusivity of the rock, respectively, s is the specific heat of the fluid, t is the time, and erfc is the complementary error function. We chose typical rock values $a = 10^{-6}$ m^2 s^{-1} and $\lambda = 2.5$ W m^{-1} °C^{-1} and used the specific heat of steam $s = 2 \times 10^3$ J kg^{-1} °C^{-1}. For $L = 10^4$ m, $Q = 2.5 \times 10^4$ kg s^{-1}, and a dike height $x = 10^3$ m, we obtain $T = 338$°C after $t = 10^6$ s. As heat continues to be removed from the dike, the vent temperature continues to decline. Because the dike cools from both sides, its width d must be great enough for thermal interference between the two sides of the dike to be negligible before $t = 10^6$ s. From the Fourier relation $at/d^2 \approx 1$, we find $d \geq 2$ m. This simple calculation indicates that a small dike can provide the heat necessary to drive megaplume flow even before thermal interaction between the dike sides becomes essential. We also ignored the latent heat of the dike.

For black smoker venting to persist after dike injection, hydrothermal circulation must be able to extract heat from a larger magma body (*13*, *20*, *24*). Moreover, the permeability of the upflow zone must decrease to a value consistent with that given by Eq. 1, otherwise the flow rate will extract heat from the magma chamber at such a great rate that the vent temperature will rapidly become small (*25*). Chemical precipitation in the cracks might reduce the permeability sufficiently (*26*).

To obtain a lower estimate of the time to seal the high-permeability zone near the dike as a result of precipitation of silica, we used the result of Lowell *et al.* (*27*) for the crack width b as a function of time in the presence of temperature and pressure gradients and assumed that the fluid composition remained in equilibrium. The expression is

$$b(x, t) = b_0 + \frac{q}{\rho_s}\frac{\partial c_s}{\partial T}\int_0^t (\partial T/\partial x)dt - \frac{\rho_f g q}{\rho_s}\frac{\partial c_s}{\partial P}t \qquad (4)$$

where b_0 is the initial crack width, ρ_f and ρ_s are the density of the fluid and the density of silica, respectively, q is the rate of mass flow per unit length of crack, $\partial c_s/\partial T$ is the dependence of silica solubility on temperature, $\partial T/\partial x$ is the temperature gradient, and $\partial c_s/\partial P$ is the dependence of silica solubility on pressure. For the set of cracks characterizing the upflow zone during megaplume flow, the dependence of silica concentration on temperature is unimportant because with closely spaced cracks (~0.1 m), the temperature of the rock and fluid in the cracks is the same within a few hours of flow. Thus, the second term on the right side of Eq. 4 is negligible. Because the solubility of silica decreases with pressure, however, silica will precipitate in cracks as the fluid ascends. Therefore, Eq. 4 becomes

$$b_0 = \frac{\rho_f g q}{\rho_s}\left[\frac{\partial c_s}{\partial P}\right]t \qquad (5)$$

from which the time t to close a crack can be found. For $b_0 = 0.0017$ m, $\rho_s = 2.5 \times 10^3$ kg m^{-3}, $\rho_f = 10^3$ kg m^{-3}, $q = 0.25$ kg m^{-1} s^{-1}, and $\partial c_s/\partial P = 10^{-11}$ Pa^{-1} (*28*), we find $t \approx 1.7 \times 10^8$ s (~5 years). This time for crack closure is a low estimate because we assumed q was constant. In reality, q decreases as the permeability decreases. Thus, it appears that high permeability at a megaplume site will persist for a long time after the megaplume event. Even if a larger magma body exists beneath the dike, the high permeability will lead to a large mass flux and rapid cooling of the magma (*25*). Consequently, according to our model, vigorous black smoker venting should not be present at megaplume sites for very long after the event occurs. Hence, our model is consistent with observations at the Co-Axial segment, where heat flux has fallen off dramatically 1 year after the megaplume events (*7*), and on the northern Cleft segment, where venting along a 17-km line of lava mounds thought to be associated with the 1986 megaplume event shut off within 8 years and perhaps much earlier (*7*).

Finally, our model is consistent with the measured ^{3}He/heat ratio (*29*) and metal content of megaplumes, which suggest that megaplume fluids are similar to equilibrium black smoker–like fluids. We suggest that when a high-temperature vent system dies (*25*), fluid circulation at temperatures of 200° to 300°C persists in the crust until venting is reinvigorated by a new episode of magma emplacement. Thus, circulating fluids will have the signature of high-temperature water-rock reaction (elevated metals), and because magma is absent, the ^{3}He/heat ratio may be less than or equal to that for typical active black smoker systems. According to our model, this reservoir of fluid (~10^8 m^3) is driven high into the water column, forming a megaplume after dike injection. On the other hand, we speculate that the lower plume results from the heating of seawater by the surface lavas, which also rapidly release ^{3}He. Thus, the ^{3}He/heat

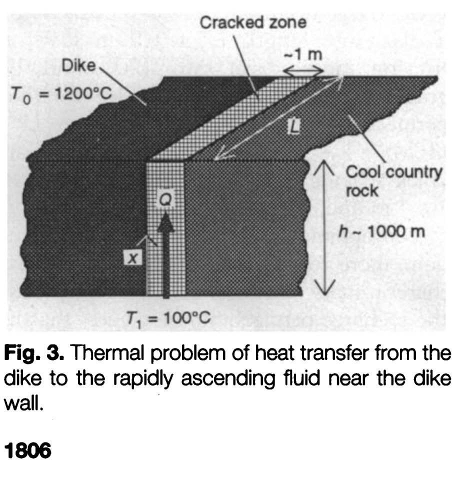

Fig. 3. Thermal problem of heat transfer from the dike to the rapidly ascending fluid near the dike wall.

ratio in the lower plume is high. Because of the higher pressure beneath the sea floor, we suspect that the ^{3}He in the dike is not released immediately but rather is partitioned into the liquid remaining in the dike interior. Upon solidification and continued hydrothermal cooling, ^{3}He from the dike may be transported to the lower plume. In the absence of additional magma, however, the ^{3}He/heat ratio there will gradually return to a lower level.

REFERENCES AND NOTES

1. E. T. Baker, G. J. Massoth, R. A. Feely, *Nature* **329**, 149 (1987).
2. E. T. Baker *et al.*, *J. Geophys. Res.* **94**, 9237 (1989).
3. E. T. Baker *et al.*, *Eos* **74** (fall suppl.), 619 (1993).
4. R. W. Embley, W. Chadwick, M. R. Perfit, E. T. Baker, *Geology* **19**, 771 (1991).
5. R. W. Embley *et al.*, *Eos* **74** (fall suppl.), 619 (1993).
6. E. T. Baker *et al.*, *Geophys. Res. Lett.* **22**, 147 (1995).
7. R. W. Embley and W. W. Chadwick, *J. Geophys. Res.* **99**, 4741 (1994); ———, I. R. Jonasson, D. A. Butterfield, E. T. Baker, *Geophys. Res. Lett.* **22**, 143 (1995).
8. J. R. Cann and M. R. Strens, *J. Geophys. Res.* **94**, 12227 (1989).
9. L. M. Cathles, *Econ. Geol.* **88**, 1977 (1993).
10. J. E. Lupton *et al.*, *Geophys. Res. Lett.* **22**, 155 (1995).
11. J. E. Lupton, E. T. Baker, G. J. Massoth, *Nature* **337**, 161 (1989).
12. E. T. Baker and J. E. Lupton, *ibid.* **346**, 556 (1990).
13. R. P. Lowell, P. A. Rona, R. P. Von Herzen, *J. Geophys. Res.* **100**, 327 (1995).
14. L. Haar, J. S. Gallagher, G. S. Kell, *NBS/NRC Steam Tables: Thermodynamic and Transport Properties and Computer Programs for Vapor and Liquid States of Water in SI Units* (Hemisphere, Washington, DC, 1984), p. 268.
15. We assume turbulent flow because of the large mass flux through a discrete number of cracks. Using the crack widths calculated from Eq. 2, we find the Reynolds number of the flow in each crack to be between 500 and 5000, which is in the turbulent regime for rough-walled cracks.
16. P. T. Delaney, D. D. Pollard, J. I. Ziony, E. H. McKee, *J. Geophys. Res.* **91**, 4920 (1986).
17. D. D. Pollard, in "Mafic Dyke Swarms," H. C. Halls and W. F. Fahrig, Eds., *Geol. Assoc. Can. Spec. Pap. 34* (1987), pp. 5–24.
18. A. M. Rubin, *J. Geophys. Res.* **98**, 15919 (1993).
19. We choose this length to be consistent with the fact that ~0.01 km^3 of magma is needed to provide the heat for a megaplume. In subsequent calculations, we assume a dike height of 1 km and show that the dike thickness must exceed ~2 m. A dike length of 10 km is not unreasonable in the light of recent observations on the Juan de Fuca, which indicate megaplume formation in conjunction with a dike propagation event of ~80 km (5).
20. M. R. Strens and J. R. Cann, *Geophys. J. R. Astron. Soc.* **71**, 225 (1982).
21. L. N. Germanovich and R. P. Lowell, *J. Geophys. Res.*, in press.
22. Calculations indicate that the boiling of seawater in isolated microcracks occurs at ≈400°C with a seafloor pressure of 20 MPa. Circumstantial evidence for this process on the sea floor comes from the magma-hydrothermal activity near 9°N on the East Pacific Rise and the apparent occurrence of hydrothermal eruption craters [R. M. Haymon *et al.*, *Earth Planet. Sci. Lett.* **119**, 85 (1993)].
23. G. Bodvarsson, *J. Geophys. Res.* **74**, 1887 (1969).
24. R. P. Lowell and P. A. Rona, *ibid.* **90**, 8769 (1985).
25. R. P. Lowell and L. N. Germanovich, *ibid.* **99**, 565 (1994).
26. Thermoelastic effects may also contribute to permeability reduction [R. P. Lowell, *Geophys. Res. Lett.* **17**, 709 (1990); L. N. Germanovich and R. P. Lowell, *Science* **255**, 1564 (1992)], but the effect occurs very quickly.
27. R. P. Lowell, P. Van Cappellen, L. N. Germanovich, *Science* **260**, 192 (1993).
28. G. C. Kennedy, *Econ. Geol.* **45**, 629 (1950); R. O. Fournier and R. W. Potter II, *Geochim. Cosmochim. Acta* **46**, 1969 (1982).
29. A linear correlation is observed between excess ^{3}He, which is attributed to magmatic degassing, and temperature anomaly (excess heat) in hydrothermal plumes, resulting in a ^{3}He/heat ratio of $\sim 0.5 \times 10^{-12}$ cm^3 cal^{-1}[gas volume given for standard temperature and pressure (STP)] for a number of vent fields in the Pacific (*11*). A similar although slightly lower ($\approx 0.3 \times 10^{-12}$ cm^3 cal^{-1} at STP) ratio is observed in megaplume fluids; however, lower level plumes observed simultaneously with the megaplume tend to have much higher values ($\sim 2 \times 10^{-12}$ to 4×10^{-12} cm^3 cal^{-1} at STP) (*11*). The values in the lower plume decline toward more normal values over time (*12*).

30. This work was supported by the NSF under grants OCE9216976 to R.P.L. and OCE9221349 and EEC-9209619 to L.N.G.

27 September 1994; accepted 18 January 1995

Diverse Effects of the Guanine Nucleotide Exchange Factor RCC1 on RNA Transport

Yan Cheng, James E. Dahlberg, Elsebet Lund*

Transport of RNAs within nuclei and through nuclear pore complexes (NPCs) are essential, but poorly understood, steps in gene expression. In experiments with mammalian cells, RCC1, the abundant nuclear guanine nucleotide exchange factor for the guanosine triphosphatase Ran/TC4, was shown to be required for nucleocytoplasmic transport of precursors of spliceosomal small nuclear RNAs (snRNAs), intranuclear transport of U3 snRNA, and processing of ribosomal RNAs, but not for export of transfer RNAs. It is proposed that guanosine triphosphate (GTP)–bound Ran/TC4 associates with ribonucleoprotein particles (RNPs) during intranuclear movement, and that GTP hydrolysis promotes deposition of RNPs at targeted sites such as NPCs or nucleoli.

Eukaryotic RNAs are generally processed in cell compartments different from those in which they function, making transport a crucial phase in their metabolism (*1*). Much remains to be learned about the mechanisms of transport of RNAs and RNPs (*2*) to and through NPCs (*3*).

An intriguing protein that appears to function in the export of mRNAs is the product of the *RCC1* gene in mammalian cells (*4*) and the homologous gene in yeast, *PRP20* (*5*), also known as *MTR1* (*6*); inactivation of RCC1 or Prp20 proteins results in accumulation of polyadenylated [poly(A)$^+$] RNAs within nuclei (*5, 6*). The RCC1 protein, originally identified in tsBN2 mutant hamster cells as a regulator of chromosome condensation (*4*), is required for many processes of mammalian cells, including initiation of DNA synthesis and progression of the cell cycle (*7*). This nuclear protein functions as a guanine nucleotide exchange factor (GEF) for the Ras-like guanosine triphosphatase (GTPase) Ran/TC4 (*8*). Although a small but significant fraction of Ran/TC4 is present in the cytoplasm where it functions in protein import (*9, 10*), the role of RCC1 in this process has not been established. Overproduction of the yeast homolog of Ran/TC4 can suppress certain *prp20/mtr1* mutations (*6, 11*), and GTP hydrolysis by this protein is needed for export of poly(A)$^+$ RNAs from nuclei (*12*); by analogy, nuclear RCC1 and Ran/TC4 may collaborate in RNA transport in higher organisms.

To investigate the role of RCC1 protein in nuclear RNA transport, we analyzed the metabolism and intracellular distribution of several other classes of RNAs synthesized in tsBN2 cells depleted of this protein (*4*). We show here that RCC1 participates in the transport of some but not all RNAs within nuclei and propose that it does so by promoting the generation of GTP-bound Ran/TC4 [(GTP)-Ran/TC4], which complexes with RNPs and allows their movement through the nucleoplasm to specific sites. The accumulation of poly(A)$^+$ or other RNAs in nuclei depleted of RCC1 would result from inefficient delivery of the RNAs to NPCs in the absence of (GTP)-Ran/TC4.

Precursors of most spliceosomal small nuclear RNAs (pre-snRNAs) undergo maturation only after they have been exported to the cytoplasm and have bound a complex of proteins, the Sm antigens (*13*). The 5′ m^{7}G-caps of pre-snRNAs are then converted to hypermethylated m^{2,2,7}G-caps and several nucleotides are trimmed off the 3′ ends before the mature snRNAs are transported back into the nucleus as snRNPs. Because small RNAs leak out of nuclei during cell fractionation (*14*), we used these cytoplasmic modifications as indicators of whether the RNAs had been exported from the nuclei of intact cells.

A shift of tsBN2 cells to the nonper-

Department of Biomolecular Chemistry, University of Wisconsin School of Medicine, 1300 University Avenue, Madison, WI 53706, USA.

*To whom correspondence should be addressed.